

Slopes, lava flow volumes, and vent distributions on Volcán Fernandina, Galápagos Islands

Scott K. Rowland¹

Hawaii Institute of Geophysics and Planetology, University of Hawaii at Manoa, Honolulu

Abstract. Digital elevation data from TOPSAR, an airborne synthetic aperture radar system that uses interferometry to derive topography, are used to determine slope distributions and lava flow thicknesses on Fernandina Volcano, Galápagos Islands. Four extracaldera slope regions are defined (from the coast inland): A coastal plain (average slope $\sim 2^\circ$), an apron (6° - 12°), steep slopes 250-600 m high (20° - 43°), and a 0.5- to 1-km-wide summit platform ($\sim 10^\circ$). Lava flows and vents are mapped using Shuttle Imaging Radar-C (SIR-C), SPOT, Landsat Thematic Mapper (TM), and air photos. Over 500 flows are identified and categorized as young, intermediate, or old based on albedo, vegetation cover, and margin preservation. By area, young flows constitute 55% of the island, 34% are intermediate, and 7% are old. The aa:pahoehoe ratio of the young flows is 85:15, whereas for the intermediate flows it is 58:42. Of the 423 vents that were classified, 236 are radial and 80% of these are in the apron, 143 are arcuate and 94% of these are in the summit platform, and 46 have transitional orientations and are about equally divided between the steep slopes and summit platform; 95% of all vents are within 13 km of the caldera center. TOPSAR data allow flow volumes to be estimated, and young flows range from <0.01 to 0.12 km³, with a total volume of 2.3 km³. By volume, 91% of the young lava erupted from radial vents below the steep slopes, many of which are concentrated within the SE apron about 5-6 km from the caldera. Similar concentrations to the NE, NW, and SW consist of young and intermediate flows. Different proportions of lava flows and vents form the different slope regions; the coastal plain averages 0.1 vents/km² and the slightly steeper apron averages 0.6 to 0.9 vents/km², increasing inland. The summit platform averages 4.7 vents/km², and this concentration supports previously proposed mechanisms for producing higher elevations and steeper slopes in the central part of the volcano. Temporal changes in the plumbing system and/or magma supply rate are suggested by the change in aa:pahoehoe ratio; it appears that in the past, low effusion rate eruptions were more common (perhaps from a filled caldera), whereas more recently, high effusion rate eruptions have dominated.

Introduction

This paper documents slopes, flow distributions, and vent distributions on Fernandina and uses these observations to make inferences about volcanic structure, subsurface plumbing, and temporal behavior, partly by comparing and contrasting with Hawaiian volcanoes.

Field reconnaissance in the 1950s, 1960s, and 1970s provides a basic framework for what is known about the Galápagos volcanoes [e.g., *Banfield et al.*, 1956; *McBirney and Williams*, 1969; *Nordlie*, 1973; *Simkin*, 1984]. Detailed recent work includes a petrological review by *White et al.*, [1993], and field studies on Floreana, Marchena, Cerro Azul, Alcedo, and Sierra Negra [*Bow and Geist*, 1992; *Vicenzi et al.*, 1990; *Nauman and Geist*, 1993; *Geist et al.*, 1994; *Reynolds et al.*, 1995]. Some recent Galápagos work has utilized remote sensing data with limited field checking [e.g., *Chadwick and Howard*, 1991;

Rowland and Munro, 1992; *Rowland et al.*, 1994]. Geophysical studies in the Galápagos have concentrated on individual events [e.g., *Filson et al.*, 1973; *Kaufman and Burdick*, 1980] or have been archipelago-wide in scope [e.g., *Case et al.*, 1973; *Feigner and Richards*, 1994]; however, none have been of sufficient spatial resolution to provide information about the internal structure of an individual Galápagos volcano.

The Galápagos Islands consist of at least 20 basaltic hotspot volcanoes ~ 1200 km west of Ecuador on the equator (Figure 1). Fernandina is a single-volcano island separated from Isla Isabela (six volcanoes) by the relatively shallow Strait of Bolivar. Fernandina has an east-west dimension of 30 km, a north-south dimension of 27 km, a subaerial area of 645 km², and a maximum elevation of almost 1470 m. The prominent caldera comprises 4% of the subaerial area. No complete geologic map of Fernandina has been published, although partial lava flows maps are presented by *Simkin* [1971], *Munro and Mouginiis-Mark* [1990], and *Munro* [1992].

Previous Galápagos studies have made particular note of the "inverted soup plate" profile [e.g., *McBirney and Williams*, 1969], and *Nordlie* [1973] produced a slope classification for the submarine and subaerial slopes. The steep upper flanks have received the most attention because it is not obvious why volcanoes that are composed almost entirely of basalt lava flows and lack obvious faults should be so steep.

¹Also at Hawaii Center for Volcanology.

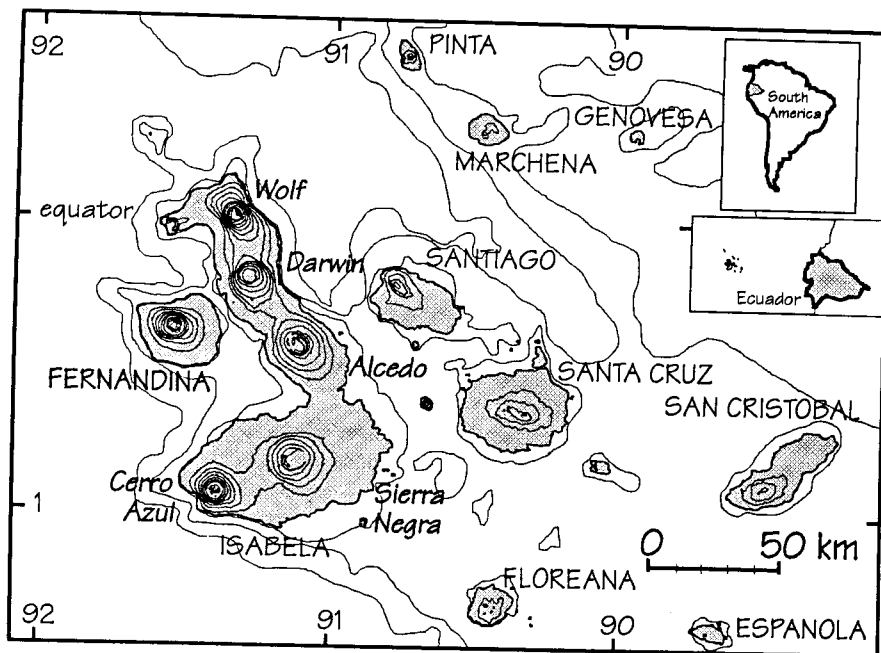


Figure 1. Location map of the Galápagos islands (adapted from a map published by *Libreria Internacional*, Quito, Ecuador). The subaerial contour interval is 200 m, and those for Fernandina and Isabela islands are from TOPSAR. Bathymetric contours (generalized) are at 100 m and then in multiples of 1000 m. Note the shallow water NE, east, and SE of Fernandina and the extension offshore of the NW topographic ridge of Fernandina.

Previous explanations for the steep slopes can be grouped into three main categories (see also discussions by *Chadwick and Howard* [1991] and *Rowland et al.* [1994]): (1) inflation of the central portion of each volcano [*McBirney and Williams*, 1969; *Nordlie*, 1973; *Cullen et al.*, 1987]; (2) preferential buildup of the central part of each volcano by either pyroclastic material or short and/or viscous lava flows [*Banfield et al.*, 1956; *Simkin*, 1972, 1984; *Chadwick and Howard*, 1991; *Reynolds et al.*, 1995]; and (3) erosion of once gradual flanks into steep sea cliffs during an eruptive hiatus [*Rowland et al.*, 1994]. Inflation would have to be permanent and very unlike that observed at monitored basaltic volcanoes, extensive amounts of pyroclastic material are not exposed in the caldera walls [*McBirney and Williams*, 1969], and the amount of erosion required might be unreasonable except at Volcán Ecuador. The better studied Hawaiian volcanic slopes and their orientations reflect the interplay of multiple construction and degradation processes [*Mark and Moore*, 1987; *Moore and Mark*, 1992], so there is no reason to suspect that a single process has produced the Galápagos volcanic forms.

The objective of this paper is to present the geology of a Galápagos volcano in sufficient detail so that the morphology and distribution of activity can provide constraints on the nature of volcanism. An additional objective is to develop appropriate methods of using remotely sensed data (including constraining their limitations) for mapping basaltic volcanoes where ground-based studies are difficult or impossible.

Data Used

One of the major problems in studying the Galápagos volcanoes has been a lack of high-resolution topographic data. Topographic maps of the Galápagos Islands originally published by the U.S. Hydrologic Office and then redistributed by the U.S. Defense Mapping Agency (DMA) have long been the only large-

scale maps available; however, they are neither complete nor accurate [*Chadwick and Howard*, 1991; *Geist et al.*, 1994]. As part of the investigation of several of the Shuttle Imaging Radar-C (SIR-C) superites, one of which is the Western Galápagos [*Mouginis-Mark*, 1995], aircraft data were collected to provide topographic data. The 1993 Topographic Synthetic Aperture Radar (TOPSAR) deployment to the Galápagos Islands was one of these missions.

TOPSAR [*Zebker et al.*, 1992; *Evans et al.*, 1992; *Mouginis-Mark and Garbeil*, 1993; *Farr et al.*, 1995] flies on the NASA DC-8 aircraft and consists of two synthetic aperture radar (SAR) antennae separated vertically by 2.6 m. This separation causes the two return signals received from each ground pixel to be out of phase; the degree to which they are out of phase depends on the distance between the airplane and the ground (at that pixel). An image consisting of the phase differences is an interferogram that can be "unwrapped" to produce a digital elevation model (DEM) with nominal 10-m spatial resolution and 1- to 5-m vertical resolution. The Fernandina TOPSAR data (Figure 2) were collected May 31, 1993, in five swaths, each 6.4 km in width. The swaths were combined into a single mosaic at the Jet Propulsion Laboratory. Unfortunately, data for the southwest tip and a 1/2-km wide strip along the northwest coast were not captured during the flight. TOPSAR data are also missing in portions of the caldera where the walls cast radar shadows. Additionally, at Cabo Douglas and Punta Espinosa it was not possible for the radar to distinguish low-lying, nearly horizontal flows from the ocean. The accuracy of the TOPSAR data can be evaluated in a number of ways: (1) comparison with topographic maps; (2) comparison with field measurements of topographic features; (3) determination of the degree of coherence between the two radar images from which the interferogram was constructed; and (4) statistical analyses of individual topographic features. The accuracy of TOPSAR data has previously been assessed by

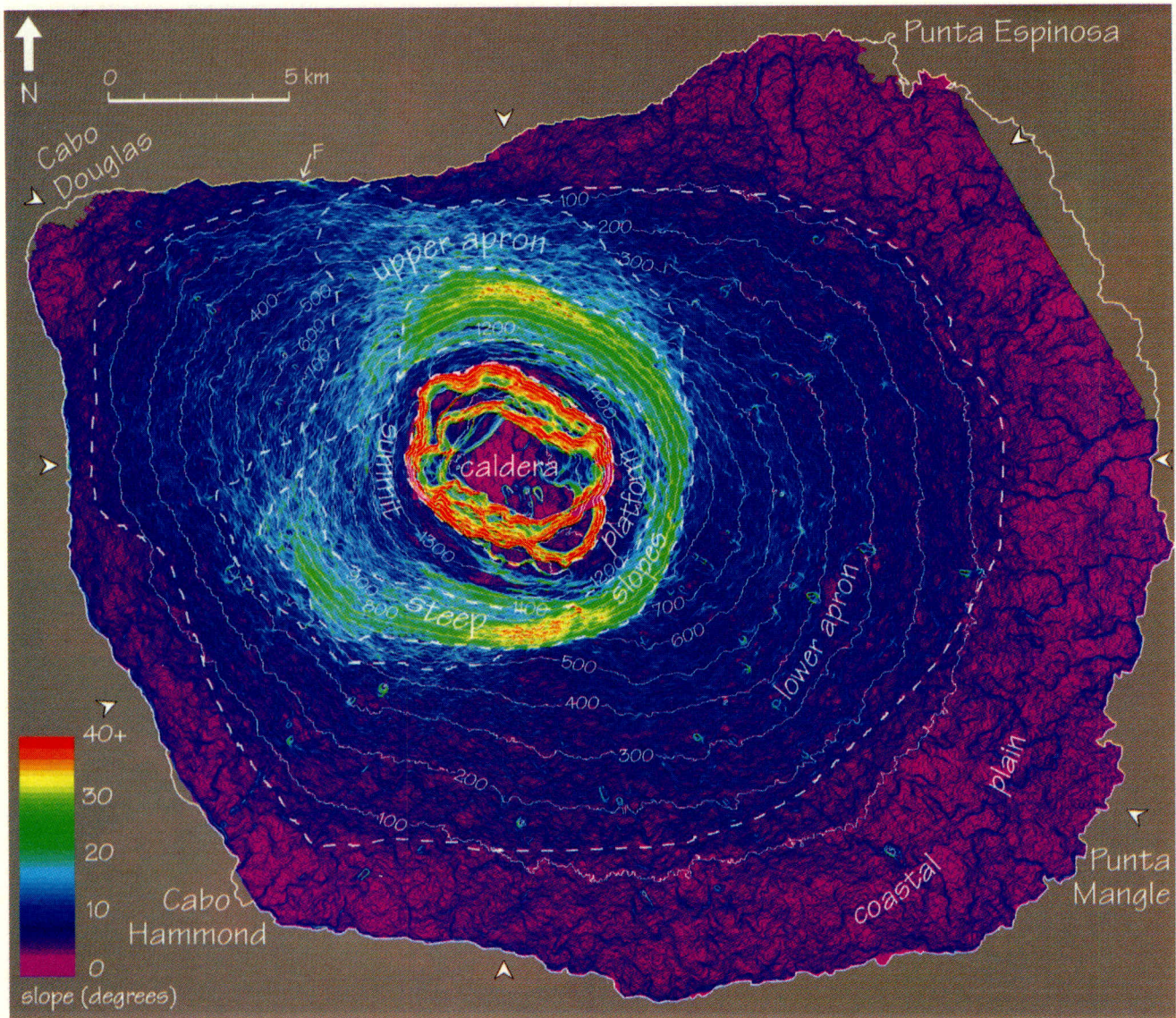


Plate 1. Slope map derived from the TOPSAR data (contour interval is 100 m). Dashed lines delimit slope regions defined in text. The steepness of the north and south steep slopes is apparent as is the abruptness of the lower boundary of the steep slopes. Note a lack of steep slopes to the NW and the encroachment of the apron against the steep slopes from NE to SE. F along the north coast indicates a possible fault. The digital elevation data were smoothed with an 11x11 median filter and a program written by H. Garbeil calculated slopes in degrees. White arrows along coastline indicate profile endpoints in Figure 3.

comparison with preexisting DEMs derived by photogrammetry [e.g., Zebker et al., 1992; Lin et al., 1994; Madsen et al., 1995].

Slopes

For the western Galápagos volcanoes, Nordlie [1973] defined gradual “subaerial lower slopes” and steep “subaerial upper slopes” and also noted a near-horizontal summit platform. The TOPSAR data (Plate 1 and Table 1) allow four subaerial slope regions to be defined, with boundaries determined by laterally continuous changes in average slope and high values of Δ slope (Figure 3; unsupervised classification schemes produced the same slope region boundaries). From the coast landward these regions are the coastal plain, the apron, the steep slopes, and the summit platform. Except from the NNW to WNW any radius constructed from the center of the caldera to the coastline will encounter all of

these slope regions, but their proportions, widths, and average slopes are not the same in all directions [Nordlie, 1973].

The inner boundary of the coastal plain is defined here as the boundary between slopes $<5^\circ$ and $>5^\circ$ and usually has an elevation of 50-150 m. The average slope of the coastal plain is $<2^\circ$ (Table 1). Local steeper slopes occur at the few vents, along flow margins, and at sea cliffs. As defined, the coastal plain is widest to the NE, east, and SE where it averages ~5 km in width, and nonexistent to the WNW and NNW.

The apron has been divided into two subregions, which together extend inland to the base of the steep slopes. The lower and upper apron subregions have average slopes of 6° and 12° , respectively. From NE to south of the caldera there is only lower apron, in places almost 9 km wide and extending inland to elevations between 900 and 600 m.

Steep slopes ranging between 16° and 43° , with an average of

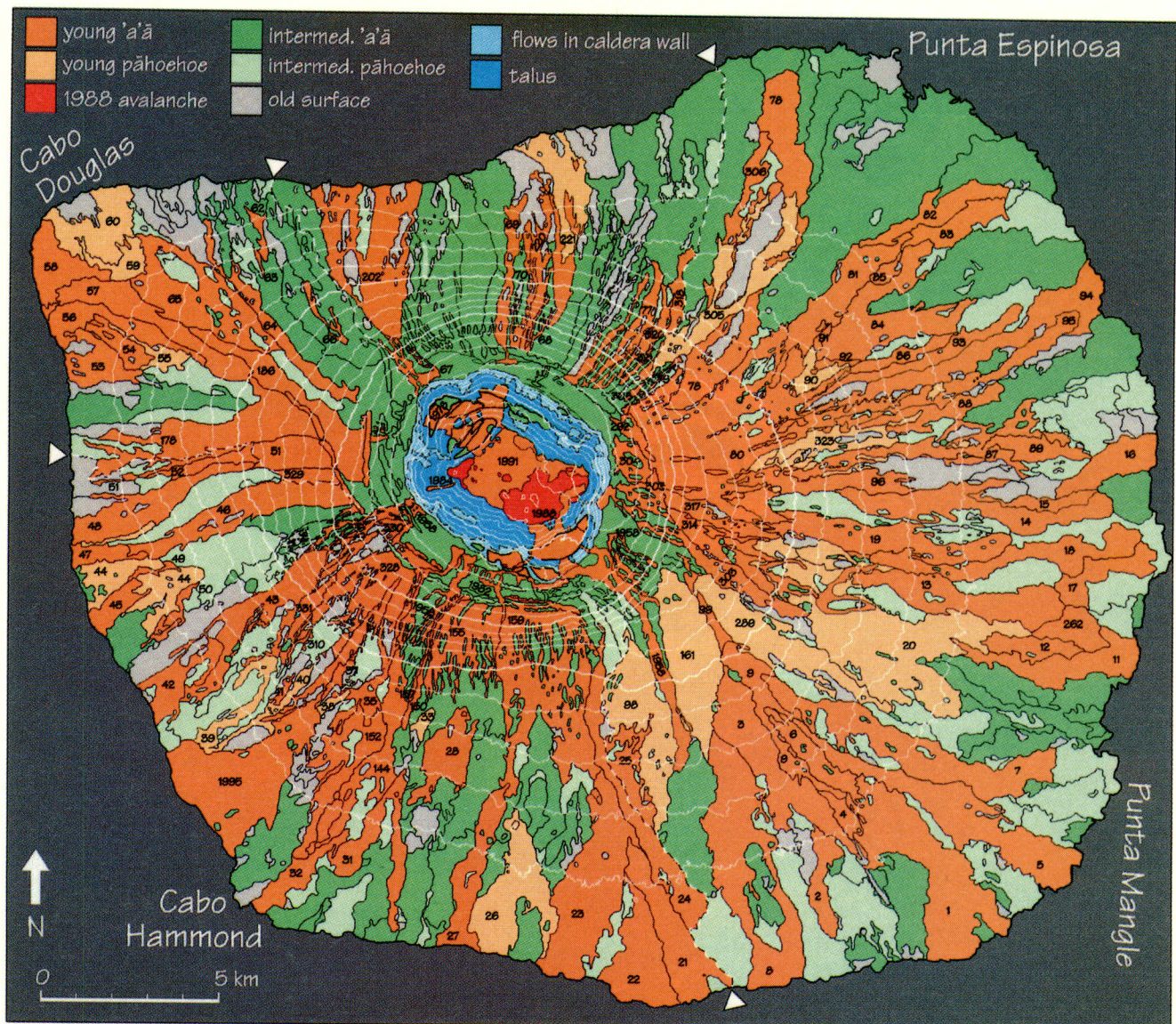


Plate 2. Surface unit map derived from all data sets. Contour interval is 100 m, and dashed lines are boundaries of flank sectors defined in text. The young lava flows are numbered, and a tabulation of area, average thickness, volume, lava type, location, and vent elevation (if known) of each of the young flows is available from the author.

20°, occur on all flanks except the NW. To the east, the lower boundary is distinct at about 900 m, and the steep slopes here are 300 m high. Clockwise to the south, the lower boundary drops to ~600 m so that the steep slopes are 600 m high. Farther west the steep slopes become less distinct, and they disappear to the NW.

The summit platform has a sharp inner boundary with the caldera walls and varies from 1 km wide in the SE to only 0.5 km towards the north and south. The summit platform dips slightly oceanward at an average slope of 6° (excluding slope contributions by identifiable vent structures). The caldera walls average 36° and the floor and prominent benches are nearly horizontal (Table 1).

Surface Units

The surface units found on Fernandina are aa and pahoehoe lava flows, vent structures (cinder and spatter cones), phreatomagmatic ash, and partially vegetated to barren soil developed on both lava and ash. Plate 2 presents the mapped flow

distributions differentiated by relative age and lava type. Most of this mapping was accomplished with a panchromatic SPOT image acquired April 27, 1988. The 10-m spatial resolution of the SPOT data is excellent for mapping lava flows [e.g., *Munro and Mouginis-Mark*, 1990], although it is not sufficient for studying noneruptive fractures or the smallest vent structures [*Chadwick and Howard*, 1991]. A Landsat Thematic Mapper (TM) image (30-m resolution) collected May 31, 1985, was used to determine some flow boundaries that were unclear in the black and white SPOT scene. A multispectral SPOT image (20-m spatial resolution) collected July 6, 1995, also proved useful for constraining unit boundaries and for mapping post-1988 eruptive units. These units include the 1988 intracaldera lava and avalanche deposit [*Chadwick et al.*, 1991; *Rowland and Munro*, 1992], the 1991 intracaldera lava flow [*Global Volcanism Network*, 1991], and the 1995 southwest flank lava flow [*Global Volcanism Network*, 1995]. All digital images were geometrically rectified to the TOPSAR data. Ancillary data included a few vertical air photos collected in 1960 (useful for mapping areas

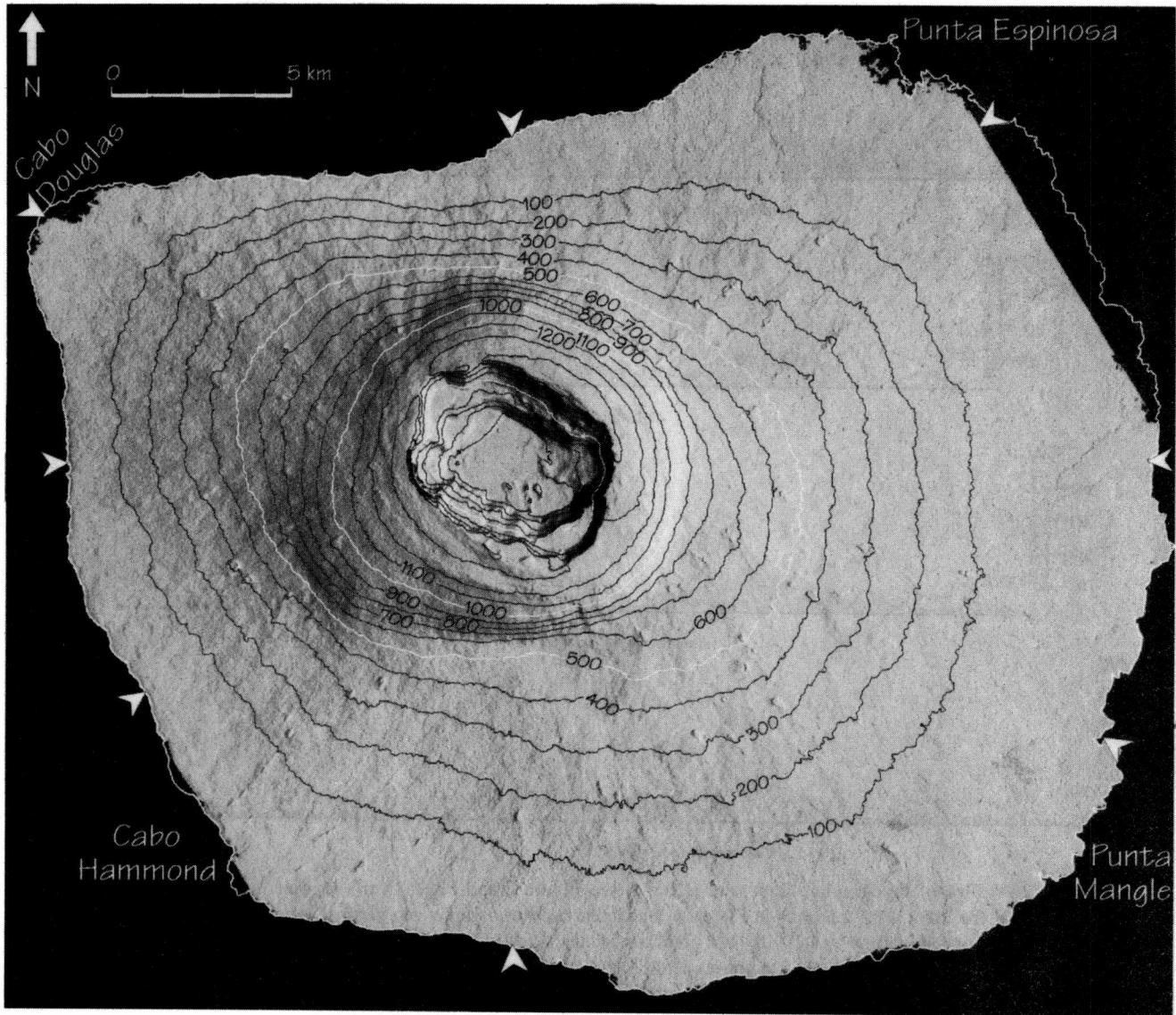


Figure 2. Shaded relief image generated from the TOPSAR digital elevation data, with pseudo-illumination from the east. The overall shape of Fernandina is highlighted, including the abrupt transition from gentle to steep flanks. Also note the numerous intracaldera benches, many of the larger radial flank vents, and the thicker lava flows on the lower flanks. It is obvious that the central high portion is offset to the north and west relative to the geometric center of the island. Arrows near coast indicate profile endpoints in Figure 3. The contour interval is 100 m, and the lowest contour within the caldera (not labeled) is 600 m. The coastline was mapped from SPOT data.

obscured by the 1968 ash), oblique air photos taken during the TOPSAR flight, and field photos and observations from September 1989.

Table 1. Slope Region Statistics

Slope Region	Percent Total Area	Average Slope, deg	Average Elevation, m
Coastal plain	40	2	43
Lower apron	41	6	296
Upper apron	6	12	481
Steep slopes	6	20	877
Summit platform	5	10	1233
Caldera walls	<1	36 ^a	974
Caldera benches	<1	3 ^b	915
Caldera floor	1	2 ^c	594

^aSome wall sections >75°.

^bExcluding talus.

^cExcluding avalanche debris.

In the absence of age dates, the lava flows were divided into three relative age classifications based on the preservation of flow boundaries and albedo. A well-preserved flow boundary shows a continuous sharp contrast with the underlying surface and rounded protrusions along its margin, particularly on downslope extensions and branches. The innumerable shadow-casting elements on young aa flows mean that regardless of the combination of viewing angle and Sun angle, the flow will appear dark in reflected light images [Campbell and Garbeil, 1991]. The albedo of pahoehoe is generally higher than that of aa, but it can be quite variable depending on the angles between the viewer, the surface, and the Sun. With time all basalt tends to oxidize (to lighter-toned reds and browns and eventually to light brown soils [e.g., Munro, 1992]), to develop vegetation (at Fernandina this can be light-toned grass or darker bushes), and to collect wind-blown or erupted pyroclastic material and dust. At Fernandina, vegetation appears to be controlled more by elevation than by flow surface

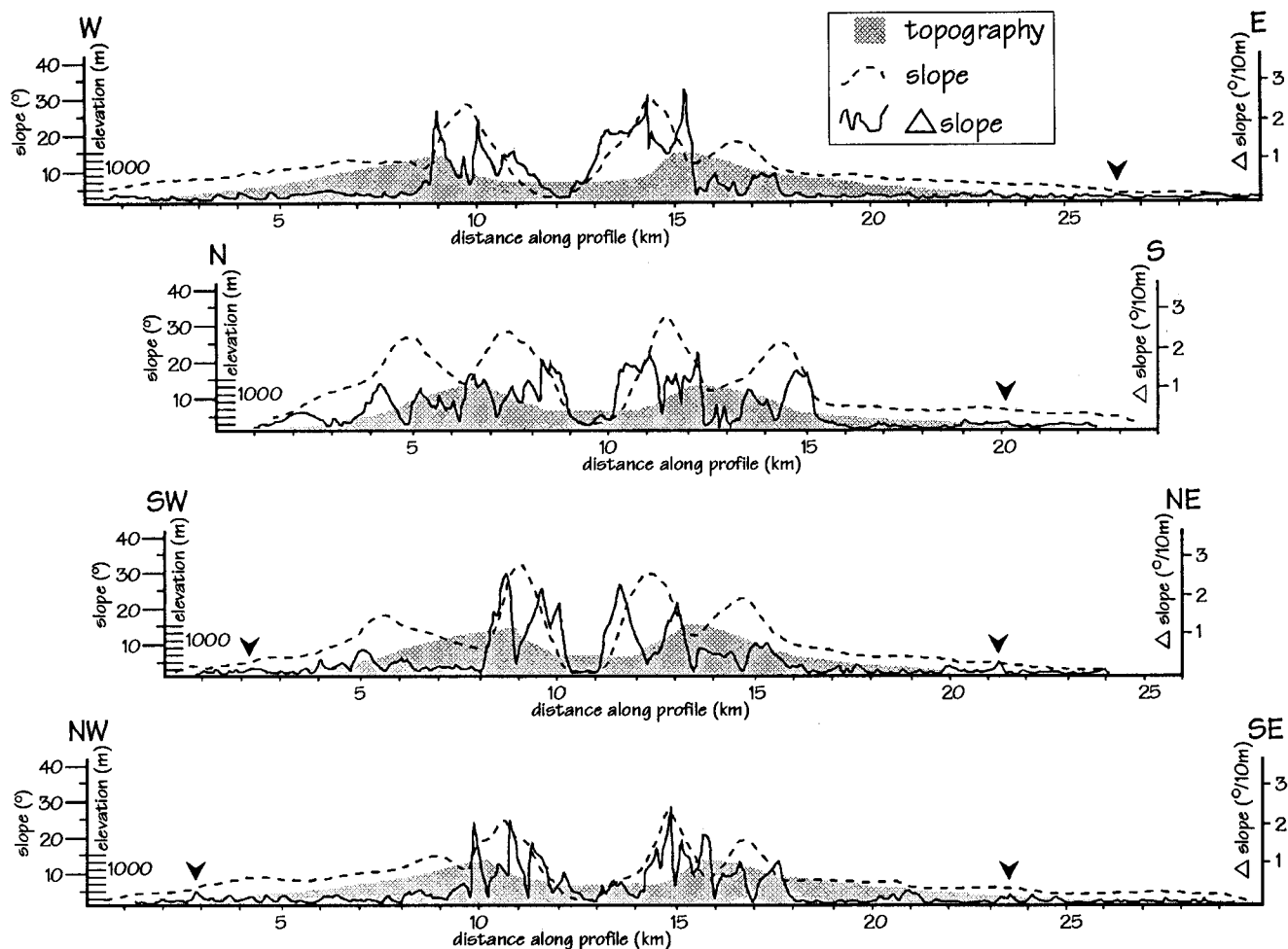


Figure 3. Profiles of topography, slope, and Δ slope (see Figure 2 and Plate 1 for endpoint locations; all profiles intersect near the letter d in "caldera" in Plate 1). Shaded area is topography (no vertical exaggeration; scale at left), dashed line is slope smoothed by a 101 by 101 pixel box (scale at left), and solid line is first derivative of slope (scale at right). Distinct slope breaks, such as the bases of the steep slopes, are obvious in all data types. The subtle boundary between the coastal plain and lower apron is indicated by small spikes in the Δ slope profiles (arrows).

age; oxidized kipukas (inliers) of old lavas near the coast support only a few scattered cacti, whereas relatively young lavas and ash near the summits may be covered by thick scrub. Relative age determinations based on albedo are thus more reliable at lower elevations where mechanical weathering is the dominant albedo-changing process.

As defined here, young flows had complete or near-complete margins, visible internal structures (pressure ridges or channels), and low albedos. Intermediate flows had margins that were cut by younger flows, margins that could not be connected to the source vent, and medium to high albedos (depending on elevation). Old

flows had outlines determined largely by the margins of younger flows, and high albedos.

In total, 564 flows were identified. Of these, 134 were classified as young, 245 as intermediate, and 185 as old, corresponding to areal percentages of 55, 34, and 7%, respectively (Table 2). A few intermediate and old flows may be parts of single flows cut by younger lava, and separate flows from the same eruption, particularly if they occur at different elevations, may have been mapped as the products of separate eruptions. The remainder of the volcano surface consists of the caldera. Presently, a 29 km² region west of the caldera is covered by the

Table 2. Surface Unit Data by Area

Unit	Area, km ²	Total Area, %	Aa		Pahoehoe	
			Area, km ²	Percent	Area, km ²	Percent
Youngest flows	358	55	304	85	54	15
Intermediate flows	220	34	128	58	90	42
Oldest flows	49	7	n.d.	n.d.	n.d.	n.d.
Caldera	25	4	n.d.	n.d.	n.d.	n.d.
Total	645 ^a	100	432	67	144	22

^aYoung intracaldera flows are included in both the youngest flows and caldera categories, but they are not counted twice in the total. Not determined, n.d.

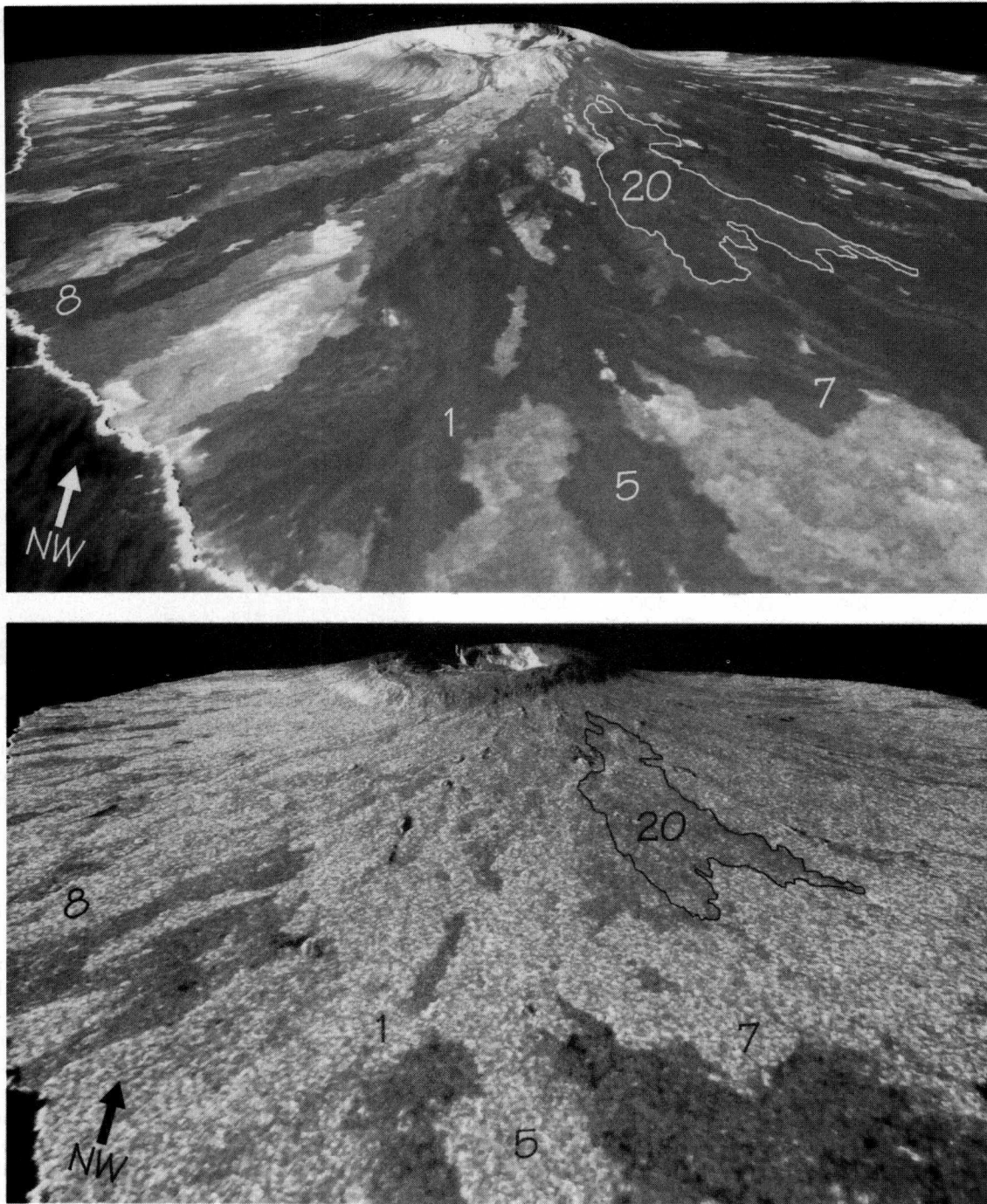


Figure 4. Perspective images of the lower SE flank just inland from Punta Mangle, produced by draping band 2 of the multispectral SPOT data (top) and the L band SIR-C data (bottom) over the TOPSAR DEM (the two data sets do not coregister exactly). In the SPOT image, flow 20 has essentially the same albedo as nearby aa lavas (8, 1, 5, and 7). However, in the SIR-C image, flow 20 produces a significantly lower return, indicating that it is smooth and thus probably pahoehoe. Prominent light-albedo, low radar-return pahoehoe flows in the foreground are of intermediate age. The view azimuth is 310° , and the viewpoint elevation is equivalent to 5000 m.

1968 phreatomagmatic ash [Simkin and Howard, 1970], but the 1960 air photos allowed vents and flows to be mapped.

Radar backscatter data provide an excellent method of characterizing surface roughness at the scale of the wavelength (for example, telling aa from pahoehoe; see, however, MacKay and Mouginis-Mark [1996]), as well as highlighting faults (if suitably oriented) and small topographic features such as cinder

cones [e.g., Drury, 1987; Elachi, 1988]. Although the general predominance of rough aa on Fernandina has been noted previously [Simkin, 1984], the SIR-C L band (24-cm wavelength) data aided in quantitative determination of aa and pahoehoe areas. Figure 4 presents portions of the SIR-C and SPOT data to illustrate how they differ with regard to different lava types. In particular, note that flow 20 has only a slightly higher albedo than

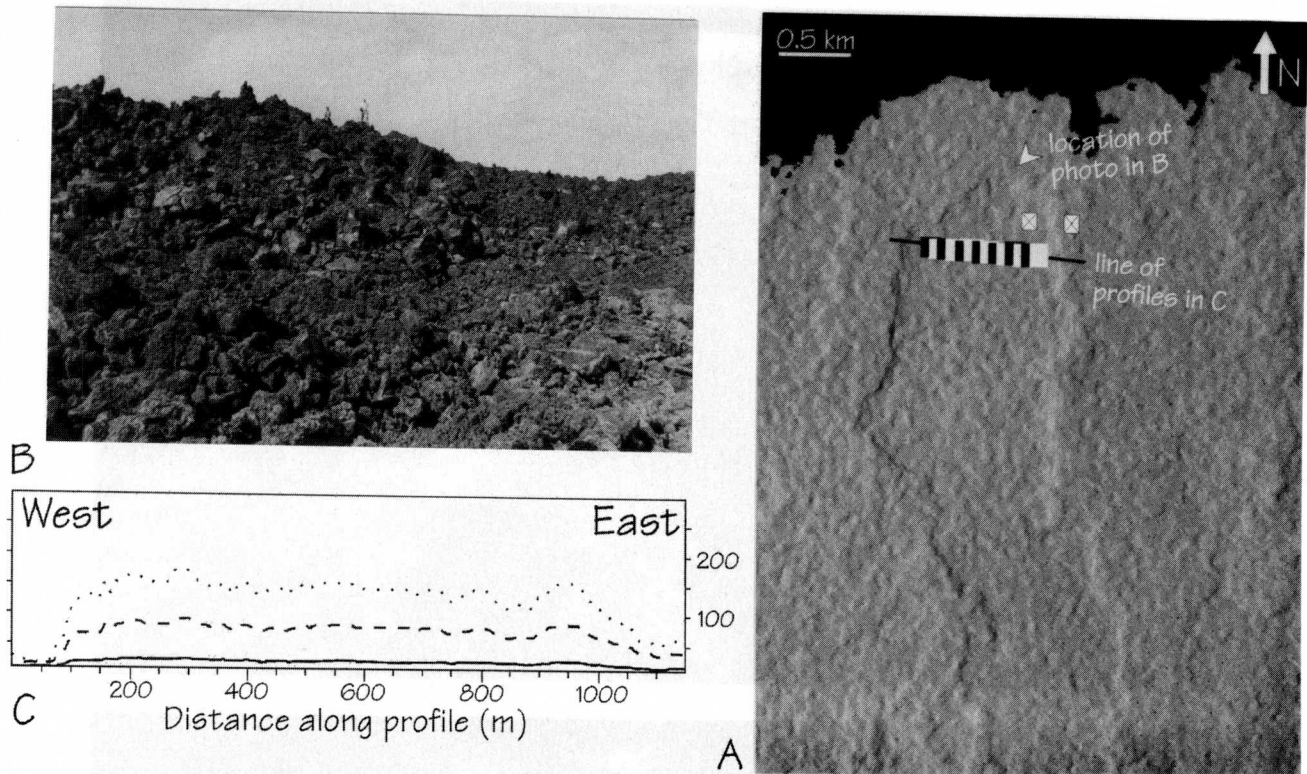


Figure 5. Various methods of assessing the accuracy of the TOPSAR data. (A) The alternating black and white boxes correspond to $\sim 10 \times 10$ pixel boxes analyzed for elevation variations and presented in Table 3 (left to right is 1-14). Arrow indicates location from which Figure 5B was taken. The solid line running under the boxes indicates the profile shown in Figure 5C, which has been drawn at no, 5x, and 10x vertical exaggeration (solid, dashed, and dotted, respectively). Average elevations in the $\sim 10 \times 10$ pixel crossed boxes yielded a thickness of 10.5 m. Note that standard deviations in Table 3 range between 0.6 and 2 m, which is on the order of the actual topographic variability seen in B.

the neighboring aa flows in the SPOT data but that in the SIR-C image, flow 20 has a low radar return, indicating that it is smooth and therefore pahoehoe.

The ability to determine flow thickness is important because inferences about subsurface plumbing and eruptive history are better constrained by lava volumes than by lava areas. To characterize the variability of the TOPSAR data at the scale of a single flow, a number of analyses were performed on the distal portion of flow 78, ~ 3 km W of Punta Espinosa (Figure 5). First, data within $\sim 10 \times 10$ pixel boxes ($\sim 10^4$ m²) were analyzed across the flow to determine the degree of variability within small areas. Table 3 shows that the standard deviation (s.d.) within the 14 boxes ranges between 0.64 and 2.02 m with an average s.d. of 1.14 m. The s.d. of all pixels along a line connecting the centers of the 14 boxes is 1.46 m. Figure 5b shows that 1-2 m of relief does exist on the flow top, but further work appears warranted in the analysis of the vertical accuracy of the data; it is not clear if real variability at the 1- to 5-m scale is being measured on aa flows or whether this is noise introduced by the radar interferometric technique. The only field measurements available were made near where Figure 5b was taken, and they yielded thicknesses of 7.5 to 9 m. A thickness of 10.5 m was calculated from the TOPSAR data by averaging elevations within 10×10 pixel boxes on and off the flow at this location. Field checking of TOPSAR data collected over Kilauea (Hawaii) indicates an accuracy of 1-2 m for aa flow thicknesses.

Flow volumes were determined with two methods, both utilizing the Interactive Topographic Analysis System (ITAS)

[Garbeil, 1993]. First, between three and seven profiles were measured on each flow along as much of the length that was identifiable. The thickness values were averaged and multiplied by the flow area to obtain a volume. At a few higher elevations, SPOT-derived flow margins could not be identified in the TOPSAR data, mainly because in such proximal locations the flows are very thin. An average thickness based on measurements of the lower part of the flow would thus not be appropriate for the whole flow. In these cases either the thickness of the nearest profile over that flow or a thickness of 2 m (typical for the proximal parts of Hawaiian flows) was assigned to the upper elevation portion in question. The second method of volume determination involved defining a reference flow base by fitting a second-degree polynomial to the vertices of a polygon corresponding to the margins of the flow. ITAS calculated the volume above the reference surface. Agreement between the two methods varied from near-exact matches (for most large-volume, unburied flows) to volume discrepancies of up to 3X (the polynomial fit method being consistently smaller). The value from the profile/area method was chosen when there was a poor agreement.

Errors in thickness will yield an uncertainty proportional to flow size. For example, the average thickness and area of flow 78 are 7 m and 8.1 km², respectively, yielding a volume of 0.056 km³. A 1.14-m s.d. produces uncertainty of ± 0.009 km³ (16%). On flow 45, however (middle of the western coastline and partially buried; average thickness and area of 3 m and 1.1 km², respectively), a 1.14-m s.d. produces an uncertainty of ± 0.001 km³

Table 3. Analysis of TOPSAR Consistency Across a Single Flow

Box	Number of Pixels	Minimum	Maximum	Mean	s.d.
1	100	20	25	22.57	1.43
2	100	19	26	22.45	2.02
3	110	19	26	22.04	1.66
4	121	21	25	22.59	1.03
5	100	21	24	22.41	0.90
6	110	21	24	22.11	0.71
7	110	21	24	22.38	0.64
8	99	19	24	21.98	1.09
9	100	19	23	21.43	1.00
10	99	19	23	21.40	0.89
11	120	19	22	20.88	1.09
12	120	19	22	20.44	1.15
13	108	19	22	20.01	1.12
14	108	18	23	19.80	1.32
Line across	76	19	24	21.64	1.46

(38%). For all flows the average thickness is 5.3 m, and the average area is 2.9 km², yielding an uncertainty of ±0.003 km³ (22%). Even with these limitations and adjustments in mind, the TOPSAR-derived flow thickness data are an extremely useful addition to this remote-sensing study. The total volume of young lava mapped on Fernandina is 2.3 km³. Of this, 83% is aa and 17% is pahoehoe. Volumes of intermediate and old lavas were not calculated.

For the purpose of discussing surface units the volcano flanks have been divided into four sectors having similar characteristic flow ages and flow sizes (Plate 2). These are the north, the NE-to-SE, the south-to-west, and the NW sectors. Because they are not equal in area, comparisons are based on percentages rather than absolute values (Table 4). The north sector of the volcano has high average slopes and a short average distance between the caldera rim and the coastline (~7 km). Young lava flows are generally small in volume and narrow. In general, this sector of the volcano is characterized by low-volume, narrow aa flows erupted from the summit platform.

The NE-to-SE coastline extends an average of 18 km from the center of the caldera. By area, 58% of this sector is covered by 51 young flows which have a cumulative volume of 1.23 km³. Six of the 10 largest young flows by volume for the entire island, and 8 of the 10 largest by area are in this sector. Although a majority of the young flows in this sector are aa, 67% and 68% of the young pahoehoe on the volcano as a whole (by area and volume, respectively) occur here. Large young pahoehoe flows erupted from radial vents at or near the base of the steep slopes.

The south to west sector of the volcano has steep slopes that become less distinct to the west. The south coastline to Cabo

Hammond averages 15 km from the caldera center, and from Cabo Hammond northward the average coastline-caldera distance is 13 km. Most of the young flows on the south flank erupted either from an extensive series of arcuate vents on the summit platform or from radial vents below 300 m.

The 1995 eruption [*Global Volcanism Network*, 1995] occurred SW of the caldera. The uppermost 1995 vents are radial and extend from 1100 down to 600 m. The volume of this upper 1995 lava is negligible. The main 1995 flow (Figure 6) erupted from a vent at around 250 m elevation and entered the ocean near Cabo Hammond, with a subaerial volume of 0.02 km³ based on an estimated average thickness of 3 m [*Global Volcanism Network*, 1995]. In total, the 1995 flow extends 9 km from the uppermost vent to the ocean and covers a subaerial area of 8.2 km². Comparison of the 1995 SPOT image with a 1992 image collected by the Japan Earth Resources Satellite-1 (JERS-1) shows no evidence for intracaldera activity associated with the 1995 eruption.

As noted above, the NW sector has the form of a broad topographic ridge and lacks steep slopes. The greatest distance from caldera to coast in this sector is almost 11 km to Cabo Douglas. Most of the lava flows in the NW sector were erupted from along the center of this broad ridge, and young lavas are concentrated at its seaward end.

Fernandina has a total area of 645 km². Of this, 55% is covered by young lavas, 33% by intermediate lavas, and 7% by the oldest surface. By area, young flows are 85% aa and 15% pahoehoe, whereas for the intermediate flows the values are 58% and 42%, respectively. Different sectors of the volcano have been more active than others at different times. For example, there are few

Table 4. Flow Data for Extracaldera Flank Sectors

Flank Sector	Young Flows			Intermediate Flows		Old Flows		Percent by Area		Young Flow Volumes, km ³	
	Area, km ²	Area, km ²	Percent	Area, km ²	Percent	Area, km ²	Percent	Aa ^a	Pahoehoe ^a	Total	Average
North	67	22	34	33	49	12	18	72	10	0.13	0.01
NE, East, SE	314	182	58	117	37	15	05	66	29	1.23	0.02
South, SW, West	155	101	65	42	27	12	08	75	18	0.59	0.02
NW	84	45	53	25	30	14	17	71	12	0.23	0.01
Total ^b	620	350	56	217	35	51	08	70	22	2.18 ^c	0.02 ^c

^aYoung plus intermediate.

^bArea total does not include caldera.

^cTotal and average volumes of young lavas including intracaldera flows are 2.2 km³ and 0.02 km³, respectively.

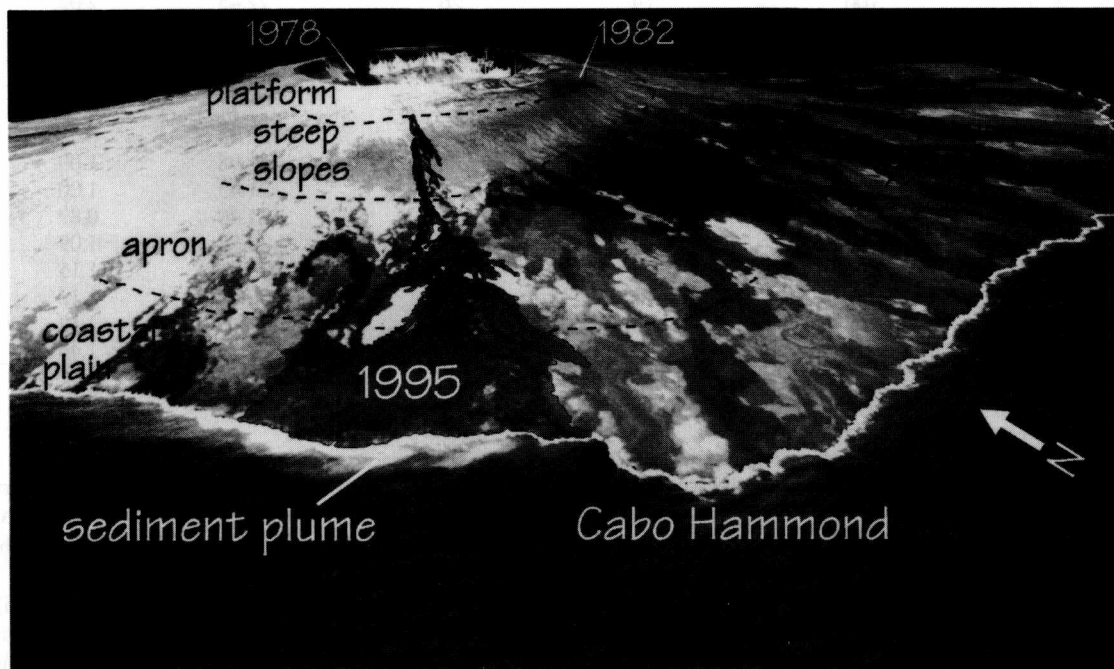


Figure 6. Oblique image of multispectral SPOT data draped over the TOPSAR DEM. The view is from the SW, showing the 1995 lava flow. Dashed lines separate slope sections. Note that the uppermost 1995 vent is just below the summit platform. Note also a plume of sediment washing northward from the new coastline formed by the 1995 flow. The view azimuth is 45° from an elevation equivalent to 5000 m.

young flows in the north sector but many in the NE-SE sector. The nature of eruptive activity is also not the same in all sectors, with young pahoehoe being concentrated SE of the caldera.

Vent Distribution

Vent maps of Fernandina have been presented by *Nordlie* [1973], *Munro and Mougins-Mark* [1990], and *Chadwick and Howard* [1991]. Most large vent structures are visible in the shaded relief, slope, and SPOT images. The largest vents are cinder cones 10 to 50 m high that occur along radial fissures within the apron. Low spatter ramparts often extend both uphill and downhill from these cones. Previously mapped smaller vents [*Chadwick and Howard*, 1991], particularly many of the 1 to 3-m-high arcuate vents on the summit platform, are generally not visible in the remote-sensing data used here. Figure 7 is therefore a compilation of vent structures mapped in the TOPSAR and SPOT and those from *Chadwick and Howard* [1991].

Vents occur on all parts of the volcano but they are not evenly distributed. Figure 7 includes a total of 423 mapped vents (compared to >435 mapped by *Chadwick and Howard* [1991]). Of these 423, 143 have a caldera-parallel arcuate orientation, 236 are radial to the caldera, and 46 are transitional between these two orientations. Table 5 summarizes the vent orientations and locations. Most of the vents are within the apron and summit platform (44% and 36% of the total, respectively), with the remaining 20% divided among the caldera, steep slopes, and coastal plain. Of all vents, 56% are radial with 81% of these located within the apron, and 33% are arcuate with 94% of these

on the summit platform. The vents with transitional orientations are about evenly divided between the steep slopes and summit platform.

Chadwick and Howard [1991] documented radial-vent concentrations to the SE, SW, NW, and NE. With the lava flow data it is possible to assign relative ages to the vent structures, which indicates, for example, that the SE concentration of radial vents has been the source for many young lava flows. On the other hand, the radial vent concentration to the NE consists of intermediate and older vents. The NW concentration (which corresponds to the broad topographic ridge) and the concentration toward the SW are about evenly divided between young, intermediate, and old vents. Most young arcuate vents are on the south summit platform and most large transitional vents are west and NW of the caldera. Nearly all subaerial vents (95%) are within 13 km of the caldera center (Figure 7) [*Chadwick and Howard*, 1991].

Figure 8 designates identifiable vent locations of young flows as circles with diameters proportional to the volume of lava produced. Recently, the most productive part of the volcano has been the upper SE apron between the elevations of 200 and 800 m. Additionally, vents near the base of the steep slopes have been the source of most of the young pahoehoe. A few moderately large flows erupted from the southern apron and coastal plain between the 80 and 200 m elevations. All other young flows are of relatively small volume.

Figure 9 differentiates the young flows by erupted volume, flow type, and vent orientation. Except for one example, all flows from arcuate vents erupted from the summit platform at elevations

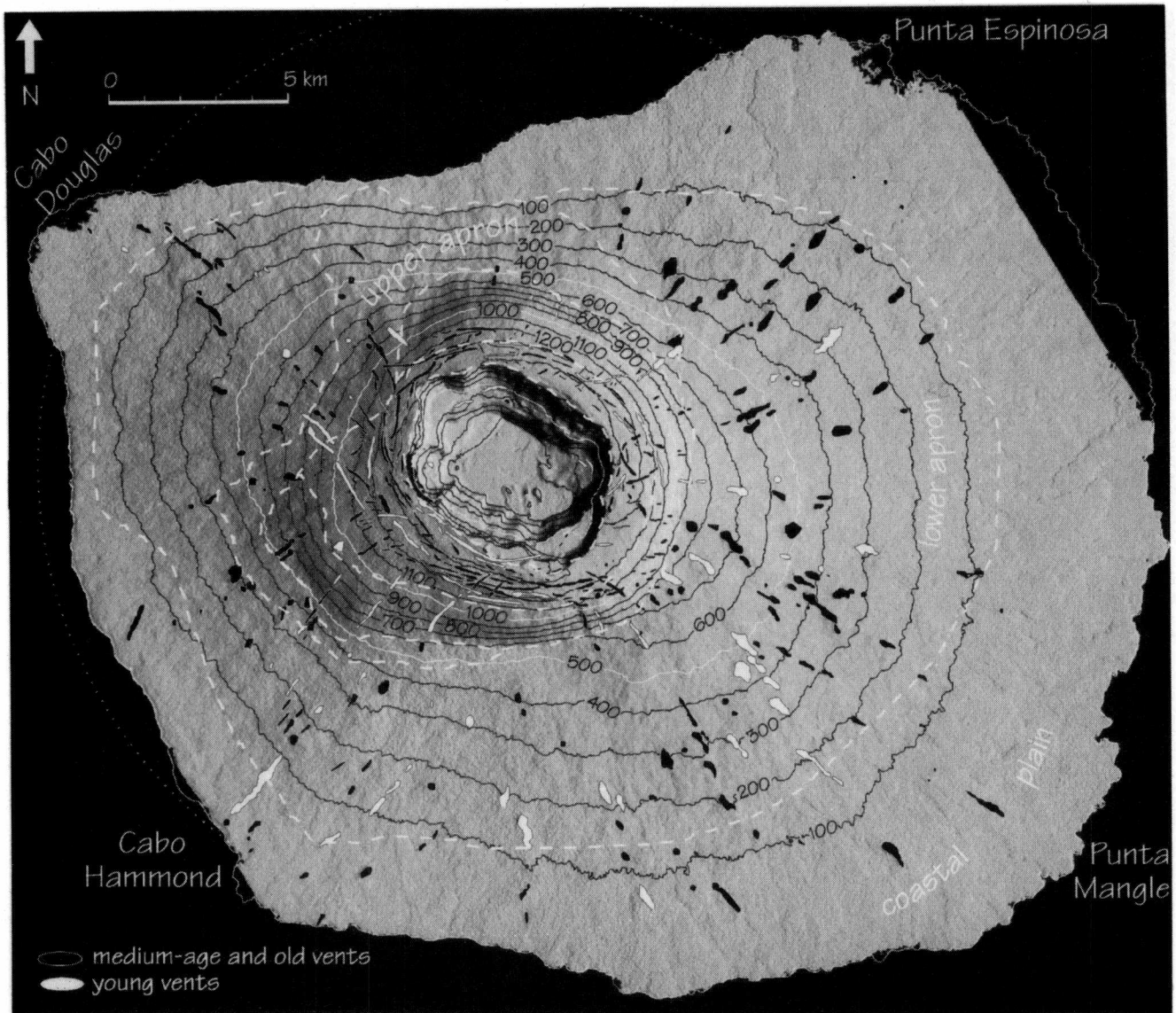


Figure 7. Vent map superimposed on a shaded relief image. Vents were mapped from SPOT and TOPSAR data and augmented with those from *Chadwick and Howard* [1991]. An attempt was made to draw the symbol at each vent location to match the extent of the actual pyroclastic construct, but for some of the narrower arcuate fissures the pyroclastic deposit is less distinct than the mapped symbol. Note the strong differentiation of vents into arcuate and radial categories. Note also that the distribution of radial vents is not uniform (see text). Dotted circle (centered on the caldera) includes 95% of all radial vents and has a radius of 13 km.

above 1100 m and have volumes less than 0.02 km³. Vents with transitional orientations mainly occur at elevations between 850 and 1100 m and supplied mostly small to moderate volumes of young lava. The great majority of radial vents occur below 1000 m and have a large range in erupted volume (up to 0.11 km³ and including all of the largest flows). Most of the young pahoehoe came from radial vents at elevations between 600 and 800 m.

Discussion

Slope Regions

The morphology of any volcano is the result of multiple constructive and destructive processes. On Hawaiian volcanoes [*Fiske and Jackson, 1972; Mark and Moore, 1987; Moore and Mark, 1992*], broad topographic ridges with slopes of 2.5°-7.5°

Table 5. Young Vent Distributions and Orientations

Vent Type	No.	Percent Total	Coastal Plain		Apron		Steep Slopes		Summit Platform		Caldera	
			No.	Percent	No.	Percent	No.	Percent	No.	Percent	No.	Percent
Radial	236	56	33	14	190	80	13	06	0	0	0	0
Arcuate	141	34	0	0	0	0	0	0	133	94	8	06
Transitional	46	11	0	0	0	0	24	52	22	48	0	0
Total	423		33	08	190	45	37	09	155	37	8	02

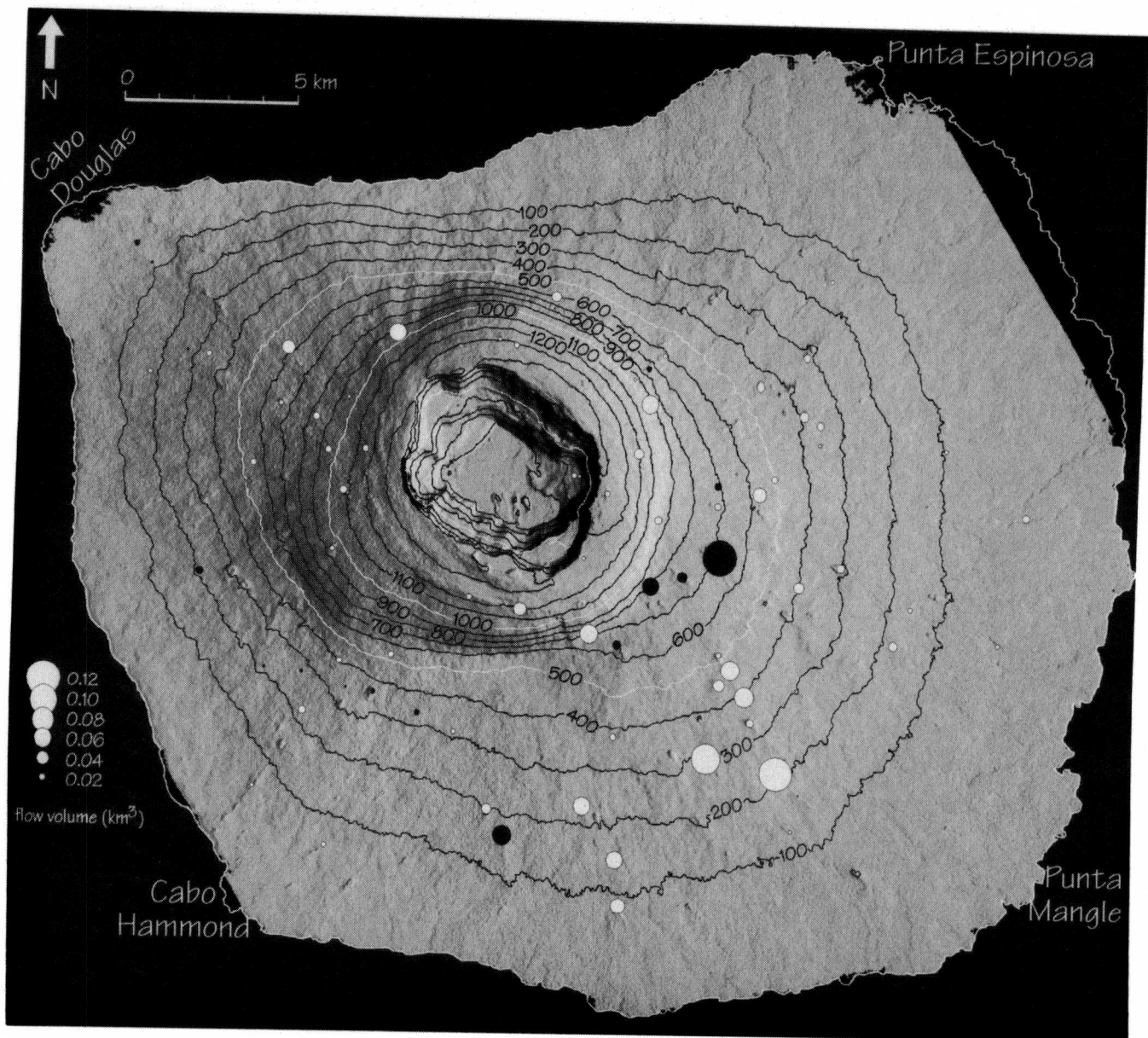


Figure 8. Vent locations of young flows mapped as circles with diameters proportional to flow volume (white, aa; black, pahoehoe; contour interval, 100 m). Note that the apron SE of the caldera has produced the highest volume of young lava, including most of the pahoehoe. There are fewer circles than young flows because some vents have been buried and because there are young flows for which vents cannot be identified.

consist of tephra and lava from zones of subparallel flank vents and define rift zones. Gentle slopes ($<2.5^\circ$) comprise either the saddles between volcanoes or coastal plains composed mainly of lava deltas [Jones and Nelson, 1970; Moore *et al.*, 1973; Mattox, 1994]. The steepest slopes (12.5° to $>22.5^\circ$) are generated by faulting or erosion and have few or no eruptive vents.

The Fernandina slope regions defined here can be attributed to different proportions of lava and vent material. The coastal plain consists almost entirely of lava flows with only a very minor amount of pyroclastic material (an average of 0.1 vent/km²). This coastal plain is thus similar to those on Mauna Loa and Kilauea which are composed of lava deltas [e.g., Moore *et al.*, 1973; Peterson, 1976; Mattox, 1994]. The Fernandina coastal plain is best developed in the NE-SE sector, corresponding to the greatest number of vents in the apron immediately inland, the largest average flow volumes (Figures 8 and 9), and the most gradual offshore slopes (Figure 1).

An increased amount of pyroclastic material in the lower and upper aprons (0.6 and 0.9 vent/km², respectively) can account for the greater slopes compared to the coastal plain. In a similar manner, the 5° - 12° slopes on the summits of Mauna Kea and Hualalai (Hawaii) are partially due to high concentrations of pyroclastic cones [Moore and Mark, 1992].

Lava and radial vents are building the apron against the steep slopes. Where there are few radial vents, the steep slopes extend to lower elevations and are being buried mainly by lavas that flowed from adjacent areas of higher production. A similar relationship was described on Volcán Wolf by Chadwick and Howard [1991] and agrees with the observations of Nordlie [1973] that at least the lower parts of the steep slopes are presently being buried rather than constructed.

The summit platform averages 4.7 vents/km², by far the highest value anywhere on Fernandina. The contribution of lava (erupted from the arcuate vents) to the summit platform and steep slopes is

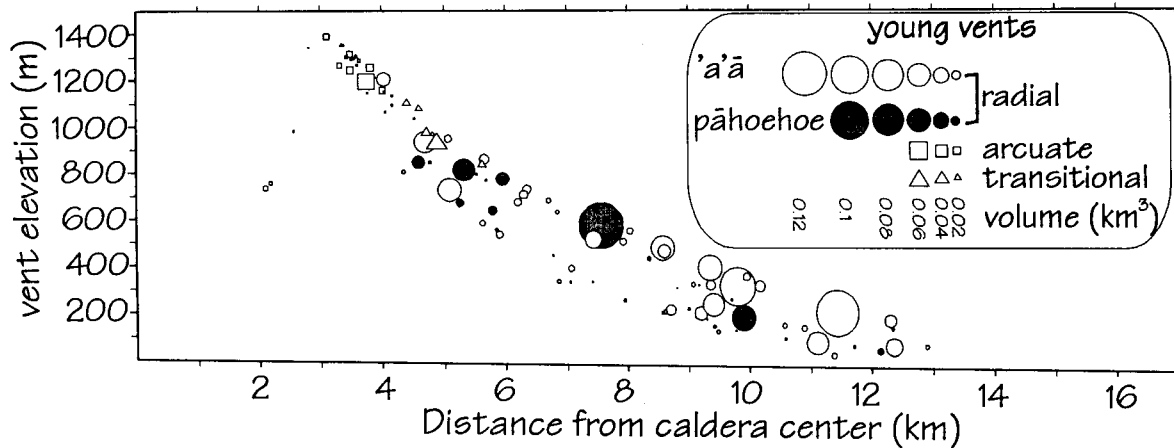


Figure 9. Graph of young vent elevation versus distance from the center of the volcano, differentiating vents by their orientation, volume of lava produced, and type of lava produced. Note that radial vents have produced the largest volume of lava, and that pāhoehoe has been preferentially produced at, or within 3 km of, the base of the steep slopes. This graph approximates a radially averaged topographic profile with a vertical exaggeration of $\sim 4X$. There are fewer circles than young flows because some vents have been buried and because there are young flows for which vents cannot be identified.

small; even the larger flows deposit most of their volume on the apron and coastal plain. The data presented here support the suggestion by *Simkin* [1984] that an annulus with a high proportion of pyroclastic material around the caldera might build upward at a rate greater than the rest of the volcano and produce the distinctive Galápagos profile.

Non-Radial Symmetry of Slope Regions

The radial symmetry of the defined slope regions is interrupted to the NW where there are no steep slopes and to the north where there is little or no coastal plain. The NW flank consists of a broad topographic ridge that is radial to the caldera and extends at least 12 km offshore (Figure 1). This also corresponds to a concentration of radial vents (Figure 9) [*Chadwick and Howard*, 1991]. Vent concentrations and a broad ridge are features of Hawaiian rift zones, but other Hawaiian rift zone features such as pit craters, open fractures, and graben are not present, suggesting that this rift zone has not developed to the extent of the Hawaiian examples.

The character of the north flank of Fernandina could be interpreted as evidence for large-scale oceanward faulting similar to that which has been described on other oceanic volcanoes [e.g., *Fairbridge*, 1950; *Moore*, 1964; *Duffield et al.*, 1982; *Moore et al.*, 1989]. This is the only part of the coastline that is concave oceanward over a long extent, and the coastal plain here is poorly developed. About 6 km east of Cabo Douglas what appears to be a 20-m-high fault downdropped toward the ocean trends inland at an azimuth of 115° (Plate 1). Regional bathymetry (Figure 1) indicates offshore slopes of $\sim 14^\circ$ to a depth of 2500 m (DMA) (D. Geist, personal communication, 1996), but the data are not sufficiently detailed to confirm or deny the presence of large-scale mass-wasting features.

Relationships Between Vent Locations, Sizes, and Slopes

The bimodal pattern of arcuate vents near the caldera and radial vents on the flanks indicates that there are two distinct stress fields [*Chadwick and Dieterich*, 1995], and the nonradial symmetry within these two populations indicates that there are perturbations

of these stresses. *Chadwick and Dieterich* [1995] also considered that there might be a feedback mechanism between these two stress regimes that would preferentially favor eruptions within one over the other at any given time. Gravitational (radial) relaxation of a roughly cone-shaped volcano will create a σ_3 that is everywhere tangential to contour lines (i.e., concentric [*McGuire and Pullen*, 1989]). Such a stress orientation will produce radially oriented dikes in all directions unless there are well-developed rift zones. Such is the case on Fernandina, although the NW, SE, and NE directions are slightly favored and the north direction is not favored).

At Hawaiian volcanoes the number of flank intrusions decreases and the average dike width increases with distance from the caldera [*Walker*, 1987; 1988], which has been attributed to the difficulty that magma pressure has in propagating dikes long distances. On Fernandina the concentration of most subaerial vents within 13 km of the center of the caldera (Figure 9) [*Chadwick and Howard*, 1991] is perhaps due to a similar limit on dike propagation. With shallower water offshore, the NE-SE coastal plain has built beyond this 13 km radius and is thus nearly devoid of eruptive vents. The vent structures produced by a basaltic eruption often consist of an elongate spatter/cinder rampart produced by the early "curtain of fire" phase and one or more larger cones produced after the eruption has localized [*Bruce and Huppert*, 1989]. At Fernandina the elongate parts of vents that are near or beyond 13 km from the caldera tend to be large, perhaps indicating wider-than-average eruptive dikes and as such providing a surface manifestation of the dike-width/caldera-distance relationship of *Walker* [1987].

The arcuate vents indicate dikes responding to a radial σ_3 . This might be due to relaxation of a "circular ridge" [e.g., *Simkin*, 1972], or perhaps mainly due to the unbuttressed caldera walls [*Munro and Rowland*, 1996]. Maintenance of a favorable σ_3 is a requirement for the longevity of vent-concentration zones [*Dieterich*, 1988]. Continued collapse of the caldera walls provides a clearer mechanism for maintaining the radial σ_3 because there is no evidence for outward movement of the steep slopes.

Although dikes orient themselves readily in a stress field

possessing a distinct σ_3 [e.g., Nakamura, 1977; McGuire and Pullen, 1989], in zones where two or more distinct stress fields interfere, dike propagation may be inhibited. At Mount Etna the 1750-m elevation is interpreted to be the boundary between volcanic flanks dominated by a regional NE-SW σ_3 below and a cone-relaxation concentric σ_3 above [McGuire and Pullen, 1989]. Around 1750 m itself, there are almost no mapped vents, and this may be due to a lack of a consistent or distinct σ_3 . Similarly, the steep slopes on Fernandina are located between a caldera-generated, inwardly radial σ_3 [Munro and Rowland, 1996] and the cone-relaxation-generated circumferential σ_3 ; interference of these two stress regimes within the region of the steep slopes may make it difficult for dikes to propagate to the surface. The common occurrence in the steep slopes of vents that are neither fully radial nor arcuate (Figure 7) [Nordlie, 1973; McBirney and Williams, 1969; Chadwick and Howard, 1991] is an additional indication that these parts of the volcano are under the influence of competing stress fields.

Temporal Variations and Supply Rates

On Fernandina a change in the style of eruptive activity from intermediate ages to recent is suggested by the areal percent covered by pahoehoe (from 42% to 15%; Plate 2 and Table 2). Additionally, intermediate-age pahoehoe is relatively evenly distributed over the whole volcano, whereas young pahoehoe is strongly concentrated in the SE apron. In Hawaii, tube-fed pahoehoe is an indication of sustained, low volumetric flow rate eruptions [Rowland and Walker, 1990] that at Kilauea also coincide with higher-than-average supply rates from the mantle [Dvorak and Dzurisin, 1993]. Long periods of sustained summit activity at Kilauea and Mauna Loa have filled the calderas and resurfaced large percentages of the flanks with tube-fed pahoehoe [Holcomb, 1987; Lockwood, 1995]. Applying these relationships to Fernandina suggests that low volumetric flow rate eruptions were more common on Fernandina in the past. Most vents of the intermediate pahoehoe are not preserved, and by analogy with Kilauea and Mauna Loa, these lavas may have overflowed from a filled caldera during a time when the magma supply rate to the volcano was higher than at present.

The total erupted volume of young lavas on Fernandina is $\sim 2.3 \text{ km}^3 \pm 0.5 \text{ km}^3$. This is a minimum value because many flows are partially buried. Although the average long-term supply rate to Kilauea has been estimated to be $\sim 3 \text{ m}^3/\text{s}$ [Swanson, 1972; Dzurisin et al., 1980, 1984], the historical surface eruption rate has been only $0.2 \text{ m}^3/\text{s}$. Using this eruption rate, the volume of young lava at Fernandina represents a time span of 365 years (± 79 years). Of course, there is no reason why the supply rates should necessarily be the same; the Galápagos hotspot is presently supplying nine active volcanoes, whereas the Hawaiian hotspot is vigorously supplying three volcanoes. The three most recent Fernandina eruptions (1988, 1991, and 1995) have a combined volume of 0.05 km^3 , which converts to an eruption rate of $1.4 \text{ m}^3/\text{s}$ during those 7 years.

The concentration of the few young pahoehoe-producing vents on Fernandina indicates that mechanically stable conduits are presently easiest to establish SE of the caldera near the base of the steep slopes. This SE direction also corresponds to one of the radial vent concentrations (Figure 7) [Chadwick and Howard, 1991] and most of the historic flank eruptions [Simkin and Siebert, 1994].

Conclusions

TOPSAR, SIR-C radar, Landsat TM, SPOT, and photographic remote sensing data have facilitated the morphological analysis of Fernandina. The ability to determine accurately the locations and values of slope regions as well as to estimate flow volumes has provided the basis for making both structural and temporal inferences.

Four slope regions were defined from the TOPSAR data and their distribution leads to interpretations of surface and subsurface activity at Fernandina. The gently sloping coastal plain consists almost wholly of lava flows and lava deltas. The apron also consists of lava flows, but the contribution of pyroclastic material causes slopes to be slightly greater. The summit platform contains the highest areal concentration of pyroclastics, which may explain how it has grown higher than the rest of the flanks, in the process generating the steep slopes [Simkin, 1984]. At present, the steep slopes are being mantled by lavas from arcuate vents on the summit platform and buried by vents and lavas of the apron.

Mapping of flows, flow types, and vents allows for an interpretation of the stress fields acting on Fernandina and records temporal changes in eruptive activity. Eruptions on the summit platform have produced small volumes of lava (average $< 0.02 \text{ km}^3$), most of which winds up on the lower flanks. Large-volume eruptions (up to 0.11 km^3) occur from radial vents mostly within the apron. Almost all young pahoehoe flows, interpreted to be associated with mechanically stable conduits, also occur on the SE apron. Most young flows are interpreted to have been erupted at high effusion rates (producing aa and cinder cones). Because almost half of the intermediate flows are pahoehoe, long-duration eruptions from mechanically stable conduits appear to have been more common in the past, perhaps associated with a filled caldera and a higher supply rate to the volcano.

This study constitutes the first detailed geologic investigation of a volcano using TOPSAR, and as such illustrates some of the benefits and limitations of the data. Further research using TOPSAR data will need to include rigorous field validation of different volcanic surfaces, employing either a laser profiler or real-time kinematic Global Positioning System (GPS) to provide an independent measure of lava flow topography. The TOPSAR data provide an important topographic baseline for quantifying future eruptive and destructive events. Although another TOPSAR mission to the Galapagos is unlikely due to the cost, topography can also be interferometrically derived from repeat passes of a single radar antenna [e.g., Gabriel et al., 1989; Massonnet et al., 1995]. Orbital radar systems such as ERS 1 and 2, JERS-1, and RADARSAT have the potential to inexpensively monitor topographic changes in the Galapagos as well as on many other volcanoes [e.g., Farr et al., 1995; Zebker et al., 1996].

Mapping of flows, vents, and slopes on Fernandina is but one step in the effort to understand basaltic volcanism in a setting other than Hawaii. Additional data that need to be collected are detailed age dates, systematic geochemical samples, and geophysical information from closely spaced seismic, deformation, and gravity networks.

Acknowledgments. This study benefited greatly from discussions with D. Munro, P. Mougins-Mark, B. McGuire, and the late V. Perez-Oviedo. Formal reviews by D. Geist, W. Chadwick, and A. McBirney were especially useful, as was an informal review by P. Mougins-Mark. I would like to thank M. MacKay, M. Robinson, and especially H. Garbeil for considerable assistance with image processing. M. Kobrick and the

crew of the NASA DC-8 aircraft are thanked for collecting the TOPSAR data, as are H. Zebker and the Radar Sciences Group at the Jet Propulsion Laboratory (JPL) for the production of the digital elevation mosaic. Air photos were kindly provided by K. Howard. This work was supported by NASA grant NAGW-1162 from the Geology Program and JPL grant 958457 from the SIR-C Program. This is SOEST contribution 4146 and HIGP contribution 913.

References

- Banfield, A.F., C.H. Bahere Jr., and D. StClair, Geology of Isabela (Albermarle) Island, *Geol. Soc. Am. Bull.*, 67, 215-234, 1956.
- Bow, C.S., and D.J. Geist, Geology and petrology of Floreana Island, Galapagos Archipelago, Ecuador, *J. Volcanol. Geotherm. Res.*, 52, 83-105, 1992.
- Bruce, P.M., and H.E. Huppert, Thermal control of basaltic fissure eruptions, *Nature*, 342, 665-667, 1989.
- Campbell, B.A., and H. Garbeil, Relations between rough surface shadowing and radar backscatter: Applications to remote sensing and spectral mixing models, paper presented at International Geoscience and Remote Sensing Symposium, Institute of Electrical and Electronics Engineers, Houston, 1991.
- Case, J.E., S.L. Ryland, T. Simkin, and K.A. Howard, Gravitational evidence for a low-density mass beneath the Galápagos Islands, *Science*, 181, 1040-1042, 1973.
- Chadwick, W.W., and J.H. Dieterich, Mechanical modeling of circumferential and radial dike intrusion on Galapagos volcanoes, *J. Volcanol. Geotherm. Res.*, 66, 37-52, 1995.
- Chadwick, W.W., and K.A. Howard, The pattern of circumferential and radial eruptive fissures on the volcanoes of Fernandina and Isabela islands, Galapagos, *Bull. Volcanol.*, 55, 259-275, 1991.
- Chadwick, W.W., T.D. Roy, and A. Carrasco, The September 1988 intracaldera avalanche and eruption at Fernandina volcano, Galapagos Islands, *Bull. Volcanol.*, 53, 276-286, 1991.
- Cullen, A.B., A.R. McBirney, and R.D. Rodgers, Structural controls on the morphology of Galápagos shields, *J. Volcanol. Geotherm. Res.*, 34, 143-151, 1987.
- Dieterich, J.H., Growth and persistence of Hawaiian volcanic rift zones, *J. Geophys. Res.*, 93, 4258-4270, 1988.
- Drury, S.A., *Image Interpretation in Geology*, 243 pp., Allen and Unwin, London, 1987.
- Duffield, W.A., L. Stieltjes, and J. Varet, Huge landslide blocks in the growth of Piton De La Fournaise, La Réunion, and Kilauea volcano, Hawaii, *J. Volcanol. Geotherm. Res.*, 12, 147-160, 1982.
- Dvorak, J.J. and D. Dzurisin, Variation in magma supply rate at Kilauea Volcano, Hawaii, *J. Geophys. Res.*, 98, 22,255-22,268, 1993.
- Dzurisin, D., S.A. Anderson, G.P. Eaton, R.Y. Koyanagi, P.W. Lipman, J.P. Lockwood, R.T. Okamura, G.S. Puniwai, M.K. Sako, and K.M. Yamashita, Geophysical observations of Kilauea Volcano, Hawaii, 2, Constraints on the magma supply during November 1975-September 1977, *J. Volcanol. Geotherm. Res.*, 7, 241-269, 1980.
- Dzurisin, D., R.Y. Koyanagi, and T.T. English, Magma supply and storage at Kilauea Volcano, Hawaii, 1956-1983, *J. Volcanol. Geotherm. Res.*, 21, 177-206, 1984.
- Elachi, C., *Spaceborne Radar Remote Sensing: Applications and Techniques*, 255 pp., IEEE Press, New York, 1988.
- Evans, D.L., T.G. Farr, H.A. Zebker, J.J. van Zyl and P.J. Mouginiis-Mark, Radar interferometry studies of the Earth's topography, *Eos Trans. AGU*, 73, 553, 557-558, 1992.
- Fairbridge, R.W., Landslide patterns on oceanic volcanoes and atolls. *The Geograph. J.*, 115, 84-88, 1950.
- Farr, T., D. Evans, H. Zebker, D. Harding, J. Bufton, T. Dixon, S. Vetrilla, D. Gesch, Mission in the works promises precise global topographic data, *EOS Trans. AGU*, 76, 225, 228-229, 1995.
- Feighner M.A., and M.A. Richards, Lithospheric structure and compensation mechanisms of the Galápagos Archipelago, *J. Geophys. Res.*, 99, 6711-6729, 1994.
- Filson, J., T. Simkin, and L.-K. Leu, Seismicity of a caldera collapse: Galapagos Islands 1968, *J. Geophys. Res.*, 78, 8591-8622, 1973.
- Fiske, R.S., and E.D. Jackson, Orientation and growth of Hawaiian volcanic rifts: the effect of regional structure and gravitational stresses, *Proc. R. Soc. London A*, 329, 299-326, 1972.
- Gabriel, A.K., R.M. Goldstein, and H.A. Zebker, Mapping small elevation changes over large areas: Differential radar interferometry, *J. Geophys. Res.*, 94, 9183-9191, 1989.
- Garbeil H., The Interactive Topographic Analysis System (ITAS), Earth Obs. System Volcanol. homepage, (<http://www.geo.mtu.edu/eos/soft/itas.html>), 1993.
- Geist, D., K.A. Howard, A.M. Jellinek, and S. Rayder, Volcanic history of Volcán Alcedo, Galápagos Archipelago: A case study of rhyolitic oceanic volcanism, *Bull. Volcanol.*, 56, 243-260, 1994.
- Global Volcanism Network, Monthly reports for March and April, Smithsonian Inst., Washington D.C., 1991.
- Global Volcanism Network, Monthly reports for February, March, and May, Smithsonian Inst., Washington D.C., 1995.
- Holcomb, R.T., Eruptive history and long term behavior of Kilauea Volcano, *U.S. Geol. Surv. Prof. Pap.*, 1350, 261-350, 1987.
- Jones, J.G., and P.H.H. Nelson, The flow of basalt lava from air into water--Its structural expression and stratigraphic significance, *Geol. Mag.*, 107, 13-19, 1970.
- Kaufman, K., and L.J. Burdick, The reproducing earthquakes of the Galapagos Islands, *Bull. Seismol. Soc. Am.*, 70, 1759-1770, 1980.
- Lin, Q., J.F. Vesecky, and H.A. Zebker, Comparison of elevation derived from INSAR data with DEM over large relief terrain, *Int. J. Remote Sens.*, 15, 1775-1790, 1994.
- Lockwood, J.P., Mauna Loa eruptive history--the preliminary radiocarbon record, in *Mauna Loa Revealed: Structure, Composition, History, and Hazards, Geophys. Monogr. Ser.*, vol. 92, edited by J.M. Rhodes and J.P. Lockwood, pp. 81-94, AGU, Washington D.C., 1995.
- MacKay, M.E., and P.J. Mouginiis-Mark, The effect of varying acquisition parameters on the interpretation of SIR-C radar data: The Virunga volcanic chain, *Remote Sens. Environ.*, in press, 1996.
- Madsen, S.N., J.M. Martin, and H.A. Zebker, Analysis and evaluation of the NASA/JPL TOPSAR across-track interferometric SAR system, *IEEE Trans. Geosci. Remote Sens.*, 33, 383-391, 1995.
- Mark, R.K. and J.G. Moore, Slopes of the Hawaiian ridge, *U.S. Geol. Surv. Prof. Pap.*, 1350, 101-107, 1987.
- Massonnet, D., P. Briole, and A. Arnaud, Deflation of Mount Etna monitored by spaceborne radar interferometry, *Nature*, 375, 567-570, 1995.
- Mattox, T.N., Where lava meets the sea: Kilauea Volcano, Hawai'i, *Earthquakes & Volcanoes*, 24, 160-177, 1994.
- McBirney, A.R., and H. Williams, Geology and petrology of the Galapagos Islands, *Mem. Geol. Soc. Am.*, 118, 197 pp., 1969.
- McGwire, W.J., and A.D. Pullen, Location and orientation of eruptive fissures and feeder-dykes at Mount Etna: Influence of gravitational and regional tectonic stress regimes, *J. Volcanol. Geotherm. Res.*, 38, 325-344, 1989.
- Moore, J.G., Giant submarine landslides on the Hawaiian ridge, *U.S. Geol. Surv. Prof. Pap.*, 501-D, 95-98, 1964.
- Moore, J.G. and M.K. Mark, Morphology of the Island of Hawaii, *GSA Today*, 2, 257-262, 1992.
- Moore, J.G., R. Phillips, R. Grigg, D. Peterson, and D. Swanson, Flow of lava into the sea, 1969-1971, Kilauea Volcano, Hawaii, *Geol. Soc. Am. Bull.*, 84, 537-546, 1973.
- Moore, J.G., D.A. Clague, R.T. Holcomb, P.W. Lipman, W.R. Normark, and M.E. Torresan, Prodigious submarine landslides on the Hawaiian ridge, *J. Geophys. Res.*, 94, 17,465-17,484, 1989.
- Mouginiis-Mark, P.J., Preliminary observations of volcanoes with the SIR-C radar. *IEEE Trans. Geosci. Remote Sen.*, 33, 934-941, 1995.
- Mouginiis-Mark, P.J., and H. Garbeil, Digital topography of volcanoes from radar interferometry: An example from Mt. Vesuvius, Italy, *Bull. Volcanol.*, 55, 566-570, 1993.
- Munro, D.C., Applications of remotely-sensed data to studies of volcanism

- in the Galapagos Islands, Ph.D. thesis, 306 pp., Univ. of Hawaii, Honolulu, 1992.
- Munro, D.C., and P.J. Mougini-Mark, Eruptive patterns and structure of Isla Fernandina, Galapagos islands from SPOT-1 HRV and large format camera images, *Int. J. Remote Sens.*, 11, 1501-1509, 1990.
- Munro, D.C. and S.K. Rowland, Caldera morphology in the western Galápagos and implications for volcano eruptive behavior and mechanisms of caldera formation, *J. Volcanol. Geotherm. Res.*, 72, 1996.
- Nakamura, K., Volcanoes as possible indicators of tectonic stress orientation--Principle and proposal, *J. Volcanol. Geotherm. Res.*, 2, 1-16, 1977.
- Nauman, T., and D. Geist, Morphologic development of Galapagos shield volcanoes: evidence from Cerro Azul, Isabela Island, *Eos Trans. AGU*, 74(43), Fall Meeting Suppl., 643, 1993.
- Nordlie, B.E., Morphology and structure of the western Galápagos volcanoes and a model for their origin, *Geol. Soc. Am. Bull.*, 84, 2931-2956, 1973.
- Peterson, D.W., Processes of volcanic island growth, Kilauea Volcano, Hawaii, 1969-1973. in *Proceedings of Symposium on Andean and Antarctic Volcanology problems*, edited by O. Gonzales-Ferran, pp. 172-189, Int. Assoc. of Volcanol. and Chem. of the Earth's Inter., Rome, Italy, 1976.
- Reynolds, R.W., D. Geist, and M.D. Kurz, Physical volcanology and structural development of Sierra Negra volcano, Isabela Island, Galápagos archipelago, *Geol. Soc. Am. Bull.*, 107, 1398-1410, 1995.
- Rowland, S.K., and D.C. Munro, The caldera of Volcan Fernandina: A remote sensing study of its structure and recent activity, *Bull. Volcanol.*, 55, 97-109, 1992.
- Rowland, S.K., and G.P.L. Walker, Pahoehoe and a'a in Hawaii: volumetric flow rate controls the lava structure, *Bull. Volcanol.*, 52, 615-628, 1990.
- Rowland, S.K., D.C. Munro, and V. Perez-Oviedo, Volcán Ecuador, Galápagos Islands: Erosion as a possible mechanism for the generation of steep-sided basaltic volcanoes, *Bull. Volcanol.*, 56, 271-283, 1994.
- Simkin, T., Geologic investigations in the Galapagos Islands during the summer of 1970, *Not. de Galapagos*, 18, 5-10, 1971.
- Simkin, T., Origin of some flat-topped volcanoes and guyots, *Mem. Geol. Soc. Am.*, 132, 183-193, 1972.
- Simkin, T., Geology of Galápagos Islands, in *Galapagos Key Environments*, pp. 15-41, Pergamon, Tarrytown, N.Y., 1984.
- Simkin, T., and K. Howard, Caldera Collapse in the Galápagos Islands, 1968, *Science*, 169, 429-437, 1970.
- Simkin, T., and L. Siebert, Volcanoes of the World, 2nd ed., 349 pp., Geoscience, Tuscon, Ariz., 1994.
- Swanson, D.A., Magma supply rate at Kilauea Volcano, 1952-1971, *Science*, 175, 160-170, 1972.
- Vicenzi, E.P., A.R. McBirney, W.M. White, and M. Hamilton, The geology and geochemistry of Isla Marchena, Galapagos Archipelago: an ocean island adjacent to a mid-ocean ridge, *J. Volcanol. Geotherm. Res.*, 40, 291-315, 1990.
- Walker, G.P.L., The dike complex of Koolau Volcano, Oahu: Internal structure of a Hawaiian rift zone, *U.S. Geol. Surv. Prof. Pap.*, 1350, 961-993, 1987.
- Walker, G.P.L., Three Hawaiian calderas: An origin through loading by shallow intrusions? *J. Geophys. Res.*, 93, 14,773-14,784, 1988.
- Zebker, H.A., S.N. Madsen, J. Martin, K.B. Wheeler, T. Miller, Y. Lou, G. Alberti, S. Vetrilla, and A. Cucci, The TOPSAR interferometric radar topographic mapping instrument, *IEEE Trans. Geosci. Remote Sens.*, 30, 933-940, 1992.
- Zebker, H.A., P. Rosen, S. Hensley, and P.J. Mougini-Mark, Analysis of active lava flows on Kilauea Volcano, Hawaii, using SIR-C radar correlation measurements, *Geology*, 24, 495-498, 1996.

S.K. Rowland, HIGP, University of Hawaii, 2525 Correa Road, Honolulu, HI 96822. (e-mail: scott@kahana.pgd.hawaii.edu)

(Received March 18, 1996; revised July 15, 1996; accepted August 27, 1996.)